Interstitial Doppler optical coherence tomography

Victor X. D. Yang, You X. Mao, Nigel Munce, Beau Standish, and Walter Kucharczyk
University Health Network, Toronto, Ontario, Canada

Norman E. Marcon
St. Michael's Hospital, Toronto, Ontario, Canada

Brian C. Wilson and I. Alex Vitkin
Department of Medical Biophysics, University of Toronto, Toronto, Ontario, Canada

Received December 20, 2004

Doppler optical coherence tomography (OCT) can image tissue structure and blood flow at micrometer-scale resolution but has limited imaging depth. We report a novel, linear-scanning, needle-based Doppler OCT system using angle-polished gradient-index or ball-lensed fibers. A prototype system with a 19-guage (diameter of ~0.9 mm) echogenic needle is constructed and demonstrates *in vivo* imaging of bidirectional blood flow in rat leg and abdominal cavity. To our knowledge, this is the first demonstration of Doppler OCT through a needle probe in interstitial applications to visualize deeply situated microcirculation. © 2005 Optical Society of America

OCIS codes: 170.4500, 170.3880, 170.3340, 170.4580, 170.3890, 170.6930.

Important biological research and clinical applications, such as detection of angiogenesis in embryological development and neoplastic transformation, monitoring of antiangiogenic therapy, and assessment of viability of transplanted organs, can benefit from high-resolution imaging of the microvasculature. Optical coherence tomography[1] (OCT) and its Doppler extensions[2,3] are being established as useful tools for visualizing tissue microstructure and microvasculature at resolutions close to cellular level, with velocity sensitivities approaching a few micrometers per second.[4–6] A key drawback of OCT is its limited imaging depth, typically 2–3 mm in most optically nontransparent tissues. Doppler OCT (DOCT) systems suffer from similar limitations, and, because of the increased signal-to-noise ratio requirement[5] for accurate velocity estimation, blood flow can rarely be detected beyond 1–2 mm from the tissue surface without *a priori* velocity profile information and extrapolation. As a result, *in vivo* DOCT imaging of human microvasculature has been restricted to a few transparent or superficial organ sites, such as the retina,[6,7] skin,[8–10] and mucosal layers of the gastrointestinal tract,[11,12] regardless of whether time- or spectral-domain OCT techniques were employed. Although the microstructure of deeper solid organs could be accessed by needle-based OCT, as demonstrated by Li *et al.*[13] with a radial sector-scanning probe, deeper microvasculature has remained out of reach with existing DOCT techniques.

In this Letter we describe a linear-scanning interstitial DOCT (IS-DOCT) needle probe that allows simultaneous visualization of tissue microstructure and microvasculature. The IS-DOCT needle is compatible with interventional radiological guidance by ultrasound (US) or computed tomography (CT) imaging. A prototype IS-DOCT needle with 0.9 mm diameter is constructed and demonstrates *in vivo* imaging of bidirectional blood flow in an animal model.

Figure 1(a) illustrates the linear-scanning IS-DOCT apparatus. The general performance of the main DOCT system and the proximal end details of the linear scanner have been described elsewhere.[5,11] Briefly, this DOCT system operates at a 1.3 μm wavelength with a coherence length of ~10 μm in tissue and can detect blood flow slower than 0.1 mm/s when imaging at 1–2 frames/s. The IS-DOCT needle probe is based on an echogenic needle commonly used in interventional radiology, which is visible interstitially under US, x-ray, or CT guidance. The IS-DOCT needle is connected via a flexible catheter to the main DOCT system, which can be positioned away from the CT gantry. Figures 1(b) and 1(c) show two designs of the IS-DOCT needle tip. Both designs employ a single-mode (SM) buffered optical fi-

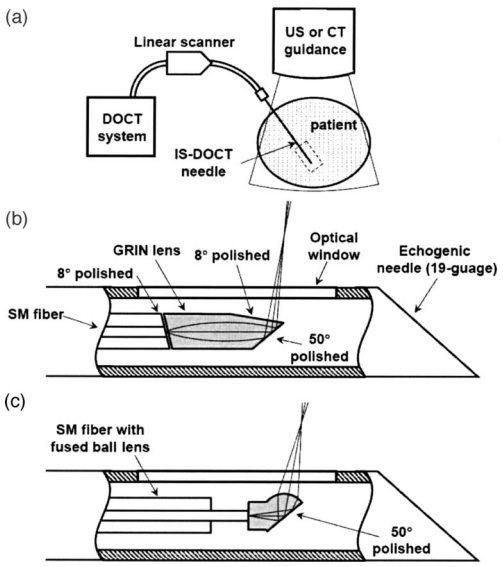

Fig. 1. (a) Schematics of the US- or CT-guided IS-DOCT and two different imaging needle designs. (b) The beam from a SM fiber is focused and deflected by a GRIN lens with three polished surfaces. (c) Simplified design with a polished ball-lensed fiber. Both designs use an echogenic needle with an optical window.

0146-9592/05/141791-3/$15.00

ber (diameter of 250 μm) that is translated along the axis of the needle by the linear scanner. In the first design, the SM fiber is polished at 8° to minimize backreflection and glued to a 250 μm diameter gradient-index (GRIN) lens that is also 8° polished at the proximal end. The distal end of the GRIN lens is polished at 50° to ensure total internal reflection and that the focused beam is reflected radially. The center length of the GRIN lens is 0.29 pitch. The beam exits through another 8° polished surface on the side of the GRIN lens. Gluing the lens and the SM fiber is performed with a micrometer positioner under orthogonal microscopy guidance (analogous to fiber splicing) with UV-curing optical cement. A flat plastic optical window is placed and secured with adhesive over a slot cut along the sidewall of the echogenic needle. Since the window reduces the effective inner diameter of the needle, a relatively large-gauge needle is used in this prototype demonstration. Rotation of the SM fiber within the needle, which is performed through the linear scanner at the proximal end of the flexible catheter, allows adjustment of the radial angular position of the exit light beam. Figure 1(c) shows an alternative approach, using a prefabricated SM fiber fused with a customized ball lens (diameter of 300 μm). The ball lens is also angle polished at 50° to allow total internal reflection, and the reflected beam is focused by the spherical surface, producing a focal spot outside the optical window. Neither design involves the use of microprisms with the intent to minimize the number of optical interfaces at the distal tip of the probe to reduce cost and backreflection, as well as to improve transmission. Both designs were ray traced using ZEMAX (San Diego, California), constructed, and tested. The second design with ball-lensed fiber was consistently easier to fabricate and was selected as the method of choice to proceed to *in vivo* demonstration.

Figure 2(a) shows a typical ball-lensed fiber after polishing, with its focal plane beam profile shown in Fig. 2(b), with a laser beam profiler (Spiricon, Logan, Utah) operating at 1550 nm. The measured beam spot sizes were 22.5 μm (y axis) and 29.3 μm (x axis), in good agreement with the ray-tracing predictions of 21.6 and 25.6 μm, respectively. The focal spot was positioned at approximately 0.8 mm from the fiber axis, outside the optical window. The asymmetry in the focal profile was due to multiple factors including spherical aberration, coma, and astigmatism, which resulted from the nonspherical shape (teardrop) of the fused ball lens and polishing depth error. Both of these must be minimized during the lens design, fusion, and polishing. In this work, the surface shape of the fused ball lens was profiled under microscopy, and the polishing depth was determined by the apparent spherical center of the intended lens surface and the fiber axis [Fig. 2(c)]. By varying the distance between the fiber end and the spherical center, the effective aperture of the lens could be designed to optimize the focal profile. During polishing, the long and short axes of the polished surface were periodically measured to ensure correct polishing depth. Multiple ball-lensed fibers were polished in house, and the

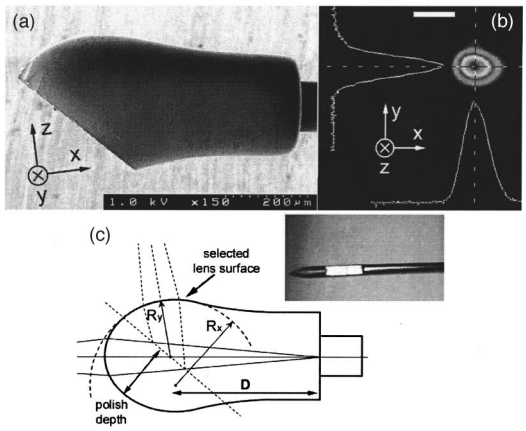

Fig. 2. (a) Scanning electron micrograph of the polished ball-lensed fiber tip. (b) Beam profile at the focal spot of the polished ball lens. The asymmetry along the x axis is likely caused by the nonspherical shape of the ball lens (scale bar=40 μm). This is illustrated in (c), where the effective radii of curvature at the selected lens surface are different in the x and y directions because of the teardrop shape. The effective aperture of the lens can be changed by varying D. The fiber tip slides inside the needle with a flat optical window (inset).

above fabrication process was reproducible.

In vivo demonstration of IS-DOCT was performed in a rat model at different anatomical locations including the thigh muscle and peritoneal cavity. The animal protocol was approved by the institutional review board. The animal was anesthetized and kept at body temperature. After the skin surface was sterilized, the needle probe was inserted as in intraperitoneal or intramuscular injection [Fig. 3(a)] and IS-DOCT images were acquired at 1 frame/s (each frame consisted of 4800 axial scans, 512 samples/scan) while under fluoroscopy guidance [Fig. 3(b)]. Tissue reflectivity, Doppler frequency shift, and variance were computed as previously[11] described, averaged over 16 sequential axial scans (with 50% overlap), and displayed simultaneously. Figure 3(c) is a typical IS-DOCT image showing bidirectional blood flow in the femoral profunda artery and vein when the needle was inserted deeply next to the femur bone. IS-DOCT could also detect changes in the blood flow [Fig. 3(d)], where external compression obliterated blood flow in the vein. Smaller blood vessels (diameter ~100 μm) could also be observed with the needle probe in the thigh muscle [Fig. 3(e)]. Finally, when the needle was inserted into the peritoneal cavity, both large and small blood vessels could be observed within the mesenteric fat [Fig. 3(f)].

In summary, we have designed and constructed a 19-gauge IS-DOCT system with *in vivo* demonstration of microcirculation imaging, which to our knowledge is the first report of DOCT visualization of deeply located blood vessels. With the current ball-lens design, the needle outer diameter could be reduced to about 0.6 mm (23–24 gauge), although flat optical window placement will be more challenging at smaller needle gauges. Further reduction of the

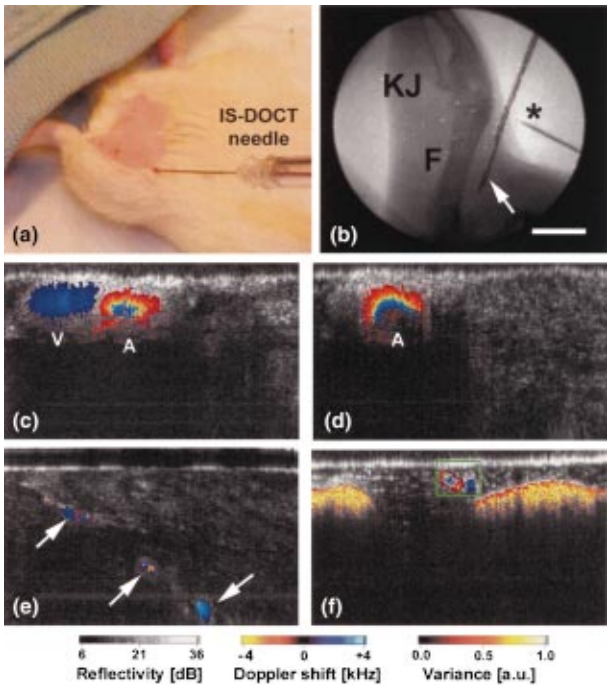

Fig. 3. *In vivo* demonstration of IS-DOCT: (a) Needle probe inserted in the thigh of an anesthetized rat. (b) Fluoroscopy showing the needle position (arrow) with relation to the femur (F) and knee joint (KJ). Another needle tip (*) marks the surface of the skin, showing that the needle is ~15 mm into the tissue (scale bar = 10 mm). (c) IS-DOCT image of an artery–vein pair, likely the femoral profunda of the rat. The flow velocity in the artery is higher, as shown by the aliasing effect. (d) Venous flow could be obliterated by compressing the vessel. (e) Smaller blood vessels (arrows, diameter of ~100 μm) were detected in the rat gluteal muscle. (f) In rat abdomen, both small and large blood vessels were detected. Because of the large velocity differences in these vessels, the larger vessels are shown with a velocity variance color scale, and the smaller vessels are shown with a Doppler shift color scale (green window). The imaging depth was reduced beneath large blood vessels, likely due to blood attenuation of the signal. The IS-DOCT image dimensions are 2.5 mm × 1.5 mm.

needle size is desirable with a smaller ball lens and custom-designed optical windows to minimize trauma to the tissue. Compared with a previous semispherical microlens design,[14] the current design allowed aperture change independent of ball-lens radius, which facilitated focus optimization. Whereas the current needle material is compatible with US, CT, or x-ray guidance, magnet-safe material can be used to fabricate an IS-DOCT probe for use with a magnetic resonance imager. Long flexible needles, inserted through the instrument channels of an endoscope, can also be used to image peri-intestinal structures under endoscopic ultrasound guidance. These different implementations will greatly expand the anatomical sites accessible to the high spatial resolution and flow velocity sensitivity of DOCT, making *in vivo* microstructural and microvascular visualization of deep tissues a possibility in the brain, liver, pancreas, kidneys, lungs, lymph nodes, breasts, or prostate. IS-DOCT may have clinical applications in providing microvascular assessment for diagnostic use or therapeutic monitoring of neoplastic diseases. For basic research, IS-DOCT may be used for imaging early cardiogenesis in small *in utero* embryos, such as mice or rats.

This work was supported by the Natural Science and Engineering Research Council of Canada, Canadian Institutes for Health Research, Canadian Foundation for Innovation, Photonics Research Ontario, Canadian Cancer Society, National Cancer Institute of Canada, and the Gordon Lang Foundation. We are grateful to the reviewers for notifying us during the submission of this Letter of a previous polished ball-lens demonstration.[15] We thank T. Liu, M. Sinclair, J. Li, and P. Herman for experimental assistance. V. X. D. Yang (victor.yang@utoronto.ca) thanks F. S. Foster, L. M. Wongkeesong, C. S. Ho, and K. Bukhanov for inspiring discussions.

References

1. D. Huang, E. A. Swanson, C. P. Lin, J. S. Schuman, W. G. Stinson, W. Chang, M. R. Hee, T. Flotte, K. Gregory, C. A. Puliafito, and J. G. Fujimoto, Science **254**, 1178 (1991).
2. Z. P. Chen, T. E. Milner, D. Dave, and J. S. Nelson, Opt. Lett. **22**, 64 (1997).
3. J. A. Izatt, M. D. Kulkarni, S. Yazdanfar, J. K. Barton, and A. J. Welch, Opt. Lett. **22**, 1439 (1997).
4. S. Yazdanfar, A. M. Rollins, and J. A. Izatt, Proc. SPIE **4251**, 156 (2001).
5. V. X. D. Yang, M. L. Gordon, B. Qi, J. Pekar, S. Lo, E. Seng-Yue, A. Mok, B. C. Wilson, and I. A. Vitkin, Opt. Express **11**, 794 (2003).
6. B. R. White, M. C. Pierce, N. Nassif, B. Cense, B. H. Park, G. J. Tearney, B. E. Bouma, T. C. Chen, and J. F. de Boer, Opt. Express **11**, 3490 (2003).
7. S. Yazdanfar, A. M. Rollins, and J. A. Izatt, Opt. Lett. **25**, 1448 (2000).
8. Y. H. Zhao, Z. P. Chen, C. Saxer, S. H. Xiang, J. F. de Boer, and J. S. Nelson, Opt. Lett. **25**, 114 (2000).
9. S. Tang, M. L. Gordon, V. X. D. Yang, M. E. Faughnan, M. Cirocco, B. Qi, E. Seng-Yue, G. Gardiner, G. B. Haber, G. Kandel, P. Kortan, I. A. Vitkin, B. C. Wilson, and N. E. Marcon, Gastrointest. Endosc. **58**, 591 (2003).
10. Y. Zhao, Z. P. Chen, C. Saxer, Q. Shen, S. Xiang, J. F. de Boer, and J. S. Nelson, Opt. Lett. **25**, 1358 (2000).
11. V. X. D. Yang, M. L. Gordon, S. Tang, N. E. Marcon, G. Gardiner, B. Qi, S. Bisland, E. Seng-Yue, S. Lo, J. Pekar, A. Mok, B. C. Wilson, and I. A. Vitkin, Opt. Express **11**, 2416 (2003).
12. V. X. D. Yang, S. Tang, M. L. Gordon, B. Qi, G. Gardiner, M. Cirocco, P. Kortan, G. Haber, G. Kandel, I. A. Vitkin, and B. C. Wilson, "Endoscopic Doppler optical coherence tomography in human gastrointestinal tract: initial experience," Gastrointest. Endosc. (to be published).
13. X. Li, C. Chudoba, T. Ko, C. Pitris, and J. G. Fujimoto, Opt. Lett. **25**, 1520 (2000).
14. S. A. Boppart, W. Luo, D. L. Marks, and K. W. Singletary, Breast Cancer Res. Treat. **84**, 85 (2004).
15. M. Shishkov, G. J. Tearney, and B. E. Bouma, *OSA Biomedical Topical Meeting* (Optical Society of America 2004), paper SE5.